Applied Catalysis B: Environmental 256 (2019) 117848

Contents lists available at ScienceDirect

Applied Catalysis B: Environmental

journal homepage: www.elsevier.com/locate/apcatb

In situ photochemical fabrication of CdS/g-C_3N_4 nanocomposites with high performance for hydrogen evolution under visible light

Lei Chen[a,b], Yiming Xu[c], Baoliang Chen[a,b,*]

[a] Department of Environmental Science, Zhejiang University, Hangzhou, Zhejiang 310058, China
[b] Zhejiang Provincial Key Laboratory of Organic Pollution Process and Control, Hangzhou 310058, China
[c] Department of Chemistry, Zhejiang University, Hangzhou, Zhejiang 310027, China

ARTICLE INFO

Keywords:
CdS/g-C_3N_4 catalyst
Photochemical synthesis
Hydrogen evolution
Heterojunction
Stability

ABSTRACT

Stable photo catalysts with high performance for hydrogen evolution under visible light are important in the field of renewable energy. Herein, a hybrid composite of CdS/g-C_3N_4 with a tunable density of CdS was made through in situ photochemical deposition of CdS nanodots onto g-C_3N_4 nanosheets. The resulting material was much more active under visible light than CdS and g-C_3N_4, not only for the photocatalytic evolution of H_2 in the presence of lactic acid but also for the photo electrochemical oxidation of water. The maximum rate of H_2 production was 2537 μmol g^{-1} h^{-1}, which was 2–10 times higher than the reported values. Importantly, the present CdS/g-C_3N_4 material was very stable during continuous irradiation for 55 h. The enhanced activity and stability are attributed to precise regulation of the position of CdS on the g-C_3N_4 surface and the formation of a type II heterojunction, increasing visible light absorption, favoring band overlapping, and promoting charge separation for interfacial reactions. This study opens a new avenue for the in situ engineering of stable photo catalysts to produce rich and active heterointerfaces for H_2 and O_2 evolution.

1. Introduction

Water splitting through semiconductor photo catalysis is an attractive method for clean energy production [1] and has been extensively studied over the past three decades [2]. To utilize solar energy, photo catalysts not only absorb visible light but also have good performance in charge separation, interfacial charge transfer, and chemical stability [3–6]. Recently, graphitic carbon nitride (g-C_3N_4) has received considerable attention because it is easily prepared and has a narrow band gap (2.7 eV) [7]. In addition, g-C_3N_4 is nonmetallic, nontoxic, and highly stable. These characteristics make g-C_3N_4 attractive for photo catalyst construction [8]. However, bulk g-C_3N_4 prepared by the conventional method has a low surface area and irregular morphology. As a result, the rate of interfacial charge transfer is not high, and the photocatalytic performance of g-C_3N_4 is poor [9,10].

To improve the photocatalytic activity of g-C_3N_4, a number of methods have been developed, including nanostructure design, heterojunction construction, doping with metal or non-metal elements, and coupling with carbon materials [11–15]. In particular, coupling g-C_3N_4 with narrow-gap semiconductors not only expands absorption into the visible light region but also improves the efficiency of charge separation [16]. As a visible-light-active photo catalyst, CdS has also received great attention [17–19]. CdS can absorb sunlight up to 560 nm and catalyze the half-reaction of water splitting to release hydrogen [20]. Moreover, CdS has a good mobility of charge carriers [21] and a variety of morphologies, including nanodots, nanospheres, nanosheets, and nanorods [22–24]. To achieve a high catalytic efficiency of CdS-based nanomaterials with the desired structures, many synthesis methods have been used, including chemical bath deposition and hydrothermal, sonochemical, electrochemical, and impregnation routes [25–31]. Coupling g-C_3N_4 with CdS may be an effective way to improve the photocatalytic activity for H_2 evolution [32–37]. Wang et al synthesized CdS quantum dots by a hydrothermal method and loaded them on g-C_3N_4 spheres [38]. This structure greatly promotes the surface kinetics of charge separation and mass transfer. Selvam et al. selected rGO as the mediator of electron transport and constructed Z-scheme hybrids (CdS/rGO/g-C_3N_4) using a hydrothermal process [39]. This Z-scheme process decreases the probability of charge carrier recombination and improves H_2 generation activity. Yin et al reported porous double-shell CdS@C_3N_4 prepared by in situ supramolecular self-assembly, which showed high photocatalytic activity and stability in H_2 production and selective oxidation of alkylarenes [40]. However, g-C_3N_4/CdS samples prepared via traditional methods (hydrothermal methods, cation exchange, etc.) suffer from serious corrosion due to the

* Corresponding author at: Department of Environmental Science, Zhejiang University, Hangzhou, Zhejiang 310058, China.
E-mail address: blchen@zju.edu.cn (B. Chen).

https://doi.org/10.1016/j.apcatb.2019.117848
Received 1 April 2019; Received in revised form 23 May 2019; Accepted 8 June 2019

hole oxidation of sulfide ions in CdS. Therefore, a suitable method of surface engineering that allows the catalyst to have ultrahigh stability while maintaining efficient hydrogen production performance is needed. A smart approach might be to precisely regulate the position of CdS on g-C_3N_4 with a controllable electronic transfer direction and particle size.

Photochemical synthesis is a gentle and rapid method for the preparation of metal (oxide) nanoparticles (NPs) on light-responsive substances. Several studies have shown that noble metals can be precisely deposited onto semiconductors through a photochemical route [41]. Under light irradiation, electrons (holes) generated by semiconductor excitation can reduce (oxidize) some metal salts into metal nanoparticles (NP) (metal oxides), which are selectively attached to specific surfaces of the semiconductor [42]. Metal (oxide) NPs (such as, Pt, Au, Ag, MnOx, and PbO_2) are often used as catalysts of semiconductor photo catalysis and have high stability against photo corrosion [43–46]. The resulting composites have the advantage of promoting charge transfer for efficient and stable hydrogen evolution [41,47–49]. Hiroaki et al reported for the first time that CdS was deposited on the surface of TiO_2 by photo deposition and proposed the formation mechanism of CdS [50]. Li et al reported the deposition of Au and CdS on the surface of g-C_3N_4 by photo deposition and constructed a Z-type heterojunction that showed excellent properties in photo degradation dye experiments [51]. In the conventional method, the CdS was randomly loaded on the surface of g-C_3N_4, by means of chemical deposition. Compared with the traditional ways, the photochemical preparation method can selectively deposit CdS on the surface of g-C_3N_4, which greatly enhanced the activity and stability of the catalyst under visible light conditions. However, no work has been found using the in situ photo deposition of CdS onto g-C_3N_4 nanosheets to precisely regulate the position of CdS with a controllable electronic transfer direction and particle size. In this study, we report such an in situ route to fabricate CdS/g-C_3N_4 nanocomposites. Under visible light, the composite materials are not only highly active for hydrogen evolution but also very stable against photo corrosion. It is proposed that CdS is photo chemically loaded onto the electron-generated sites of g-C_3N_4 with the formation of a type II heterojunction.

2. Experimental

2.1. Material preparation

Bulk g-C_3N_4 nanosheets were prepared by following a previous report [5]. Briefly, 10 g melamine was heated at 550 °C under air for 4 h with a ramp rate of 2.3 °C min^{-1}. Then, yellow bulk g-C_3N_4 was milled into a fine powder and further treated at 500 °C under air for 2 h with a heating rate of 5 °C. CdS/g-C_3N_4 was prepared by a photochemical method. An ethanol suspension (200 mL) containing 200 mg g-C_3N_4 was mixed with S_8 (64 mg) and $Cd(NO_3)_2{\cdot}4H_2O$ (1.23 g). The suspension was purged with N_2 for 30 min and then irradiated with a 300 W Xenon lamp for 1, 2, 3, 4, and 5 h. Then, the bright yellow product was collected by centrifugation, washed several times with water and ethanol, and dried at 60 °C overnight. The resulting samples are denoted as CS-*x*, where *x* represents the time (hours) used for the photochemical deposition of CdS (Table 1). Pure CdS was made according to the previous literature [32]. $Cd(NO_3)_2{\cdot}4H_2O$ (8 mmol), thiourea (8 mmol), and polyvinylpyrrolidone (0.9 g) were dissolved in 80 mL water. Then, the solution was transferred into a Teflon-lined autoclave (100 mL) and heated at 160 °C for 12 h in an oven. After that, the solid was collected by centrifugation, washed with ethanol and water several times, and dried at 60 °C overnight.

Table 1
Contents of Cd and CdS in CdS/g-C_3N_4 samples measured by AAS.

Catalysts	Irradiation time (h)	Cd (wt%)	CdS (wt%)
CS-1	1	2.73	3.50
CS-2	2	11.29	14.50
CS-3	3	16.10	20.68
CS-4	4	19.93	25.60
CS-5	5	23.22	29.83

2.2. Solid characterization

Scanning electron microscopy (SEM) was performed on an SU-8000 (Hitachi, Tokyo). Transmission electron microscopy (TEM) was performed on an FEI Tecnai G2 F20 S-TWIN (FEI, America). X-ray photoelectron spectroscopy (XPS) was conducted on an Escalab 250 Xi (America) with an Axis Ultra DLD spectrometer (resolution 0.5 eV). X-ray diffraction (XRD) patterns were recorded on a D8 Advance (Bruker, Germany) with Cu Kα radiation. UV–vis diffuse reflectance spectra (DRS) were recorded on a TU-1901 UV–vis spectrophotometer (Pgeneral, China) equipped with an integrating sphere and with $BaSO_4$ as a reference. Photoluminescence (PL) spectroscopy was performed on an FLS920 spectrophotometer (Edinburgh, UK) equipped with a xenon lamp. The surface functional groups were examined using Fourier transform infrared spectroscopy (FTIR, Nicolet, America). N_2 adsorption was measured at −196 °C on a NOVA-2000E analyzer and used to calculate the Brunauer-Emmett-Teller (BET) surface area.

2.3. Photo catalysis

Photocatalytic reactions were carried out on a water-splitting apparatus (Labsolar-6A, Perfect Light Beijing). Prior to irradiation, a suspension (100 mL) containing 20 mg catalyst and 10 vol.% lactic acid was evacuated several times to completely remove air. After that, the vessel was vertically irradiated at 6 °C with a 300 W Xe lamp (Microsolar AR300, Perfect light, Beijing) equipped with a 420 nm cut-off filter. When necessary, the catalyst was photo chemically deposited with 1 wt% Pt from a H_2PtCl_6 solution. The amount of H_2 released in the vessel was analyzed by a gas chromatograph (9790 II, Fuli, Zhejiang) equipped with a thermal conductivity detector (TCD). The amount of Cd^{2+} dissolved in solution was analyzed by atomic absorption spectroscopy (AAS, PerkinElmer, USA).

2.4. Photo electrochemical measurements

A working electrode was prepared as follows. First, 2.0 mg of catalyst was dispersed in a solution containing 1 mL DMF (N,*N*-dimethylformamide) and 20 μL Nafion perfluorinated resin. Then, 20 μL of the suspension was uniformly dropped onto a 0.5 × 0.5 cm^2 indium-tin oxide (ITO) glass and dried at 60 °C overnight. Measurements were performed on a CHI600D electrochemical analyzer (Chenhua Instruments Co., Shanghai) in a standard three-electrode system, with a Pt wire as the counter electrode and Ag/AgCl as the reference electrode. The electrolyte was 0.50 M $NaClO_4$ (pH 6.7), and the light source was a 300 W Xe lamp.

3. Results and discussion

3.1. Solid characterization

Fig. 1 shows the XRD patterns of the samples. For g-C_3N_4, there were two distinct diffractions, corresponding to the in-plane structural packing motif and interlayer stacking of aromatic segments for graphitic materials, respectively [33]. For CdS, there were six major peaks with lattice constants of a = 4.1307 Å and c = 6.7144 Å, well matching those for hexagonal CdS (JCPDS: 41–1049) [32]. For CdS/g-C_3N_4, the characteristic diffractions of g-C_3N_4 and CdS decreased and increased, respectively, as the irradiation time for CdS formation increased. These observations indicate that CdS was successfully deposited onto g-C_3N_4 without changing the crystal structure.

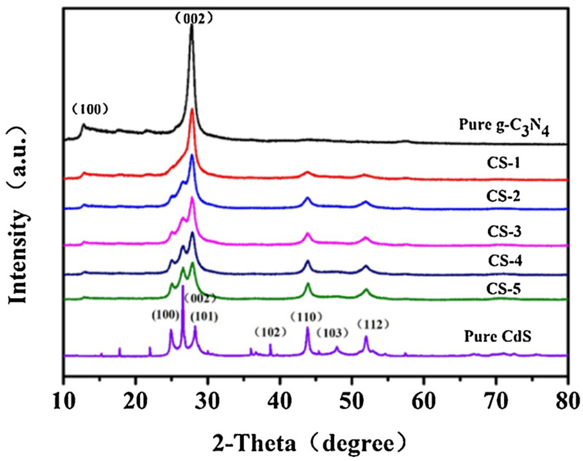

Fig. 1. XRD patterns of the samples as indicated by the legends. CS-x represents the CdS/g-C_3N_4 sample prepared from the photochemical deposition of CdS onto g-C_3N_4 for x h.

Fig. 2 shows the SEM and TEM images of the samples. Pure g-C_3N_4 had a two-dimensional layer structure with a thickness of approximately 1–10 nm, and the surface was smooth and wrinkle-free (Fig. 2a). Pure CdS was in the form of nanodots, which were tightly aggregated into an irregularly large-sized particle (Fig. 2b). The image of CS-4 shows many fine particles of CdS separately and uniformly deposited on the surface of g-C_3N_4 (Fig. 2c). The particle size of CdS on g-C_3N_4 was smaller than 20 nm. The TEM and HRTEM images showed that CdS selectively attached to the surface of the g-C_3N_4 nanosheets (Fig. 2d), whereas the lattice fringes of 0.311 and 0.330 nm corresponded to the (101) and (002) planes of CdS, respectively (Fig. 2f). Interestingly, there was intimate contact between CdS and g-C_3N_4, which was beneficial to charge transfer between the two materials. STEM-EDX mapping showed that all elements (C, N, Cd, and S) were uniformly distributed in CdS/g-C_3N_4 (Fig. 2g). These observations indicate that the sample prepared by the photochemical deposition of CdS onto g-C_3N_4 possesses a heterostructure and is not simply a physical mixture of two separate phases (g-C_3N_4 and CdS).

Fig. 3a shows the FTIR spectra of the samples. Pure g-C_3N_4 had three absorption regions. The broad band from 3000-3400 cm^{-1} is assigned to the stretching vibrations of terminal –NH_2 or –NH groups (3201 cm^{-1}) at the defect sites of aromatic rings [52]. The absorption peaks at 1200-1700 cm^{-1} are the typical stretching modes of aromatic carbon nitride heterocycles, whereas the band at 812 cm^{-1} is due to the characteristic breathing mode of s-thiazine units. All of these peaks were also observed in CS-4. For pure CdS, the broad absorption peaks at 3430 cm^{-1} and 1632 cm^{-1} are attributed to surface-adsorbed water. The peaks at 2062 cm^{-1}, 1387 cm^{-1}, 1100 cm^{-1}, and 616 cm^{-1} can be attributed to Cd-S bonds [36]. These peaks were also observed in CS-4. These observations indicate that the structure of g-C_3N_4 remains unchanged upon CdS deposition.

XPS was used to examine the chemical composition of CS-4. C, N, S, Cd, and O were all present in the sample (Fig. 3). The small quantities of O observed are due to the adsorbed H_2O and CO_2 on the solid surface. The XPS spectrum of C 1s can be deconvoluted into three peaks (Fig. 3c). The peak at 284.6 eV is ascribed to graphitic carbon-carbon bonds. The peak located at 287.9 eV corresponds to sp^2-bonded carbons in the N-containing aromatic structure (N—C = N). The weak peak at 285.9 eV is attributed to sp^3-bonded carbon species from defects in the g-C_3N_4 surface [52]. The high-resolution XPS spectra of N 1s showed three peaks (Fig. 3d). The main peak at 398.8 eV is assigned to sp^2-bonded nitrogen in the thiazine ring (C–N = C). The other two peaks at 400.1 and 401.2 eV are assigned to tertiary nitrogen-bonded carbon (N – $(C)_3$) and amino groups with a hydrogen atom (C—N—H), respectively [52]. The XPS peaks of Cd 3d at 404.9 and 411.6 eV (Fig. 3e) are assigned to Cd $3d_{5/2}$ and $3d_{3/2}$, respectively, as observed for CdS [53]. The peaks of S 2p at 161.2 and 162.4 eV (Fig. 3f) are ascribed to S^{2-} in CdS [35]. XPS analysis further confirms that CdS was photochemically deposited onto g-C_3N_4, in agreement with the above results (Fig. 2).

Fig. 4a shows the adsorption↓desorption isotherms of N_2 on g-C_3N_4 and CS-4. The isotherm was type IV, indicative of a mesoporous

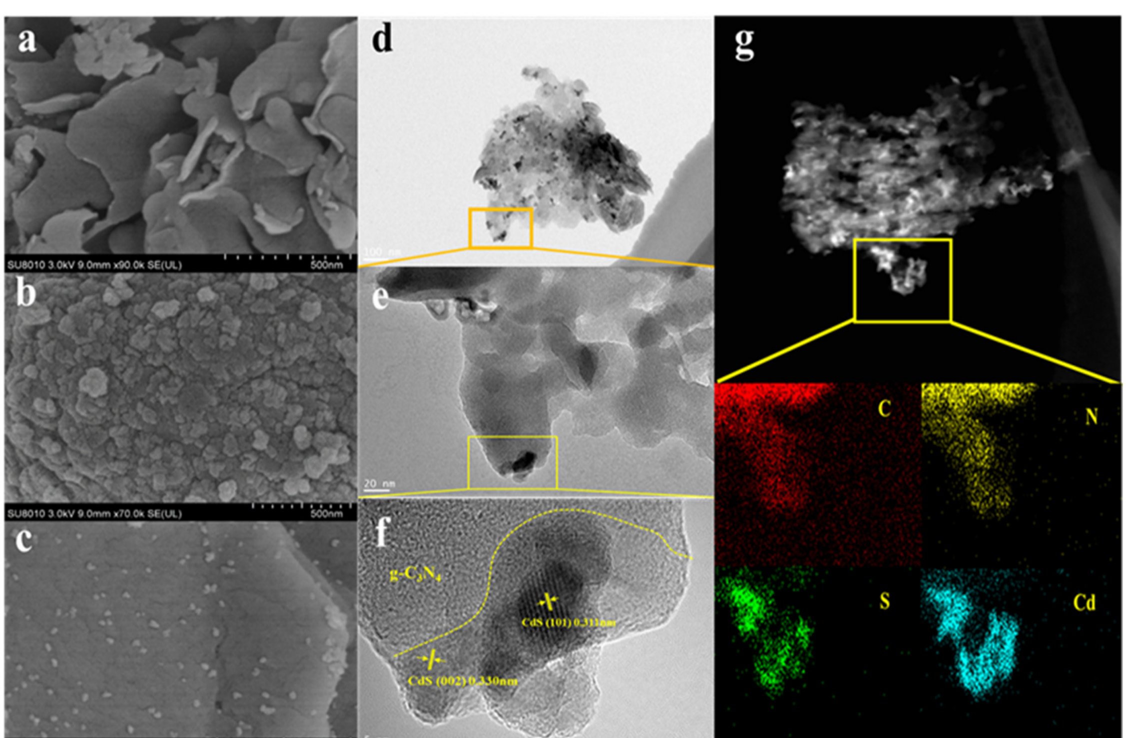

Fig. 2. SEM images of g-C_3N_4 nanosheets (a), CdS (b), and CS-4 (c). TEM (d, e) and HRTEM (f) images of CS-4. STEM-EDX elemental mapping of CS-4 (g).

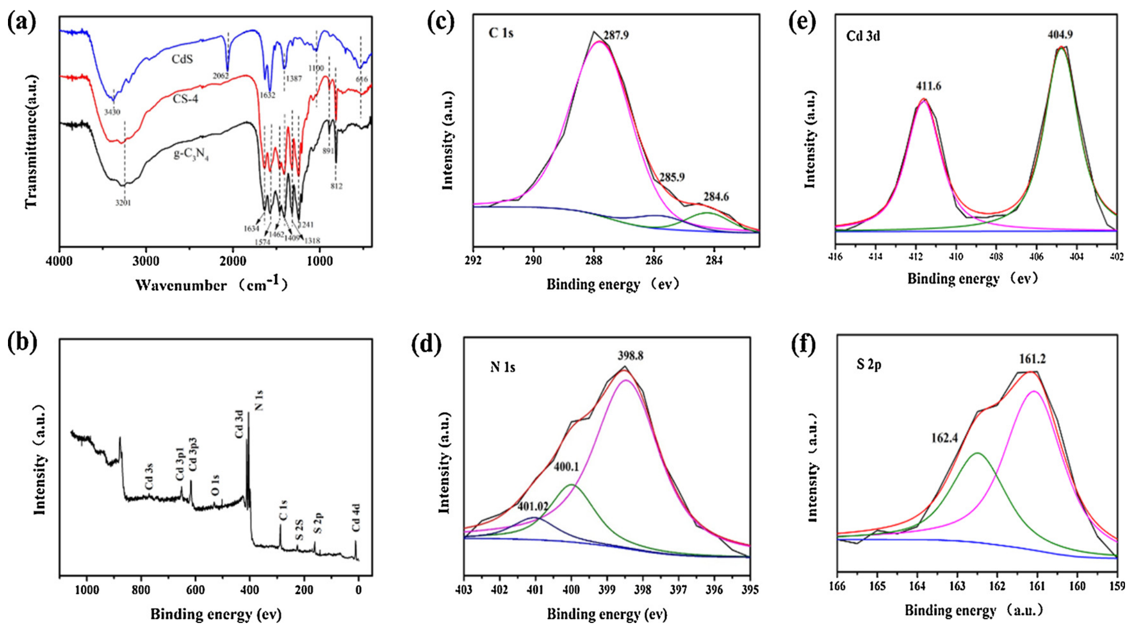

Fig. 3. FTIR spectra of g-C_3N_4, CdS and CS-4 (a). XPS spectra of CS-4 (b) and the corresponding high-resolution XPS spectra of C 1s (c), Cd 3d (d), N 1s (e), and S 2p (f).

structure. The BET surface areas of g-C_3N_4 and CS-4 were calculated to be 127 and 115 $m^2\,g^{-1}$, respectively. Two samples had similar average pore sizes of 3.0 nm (Fig. 4b). However, in the pore size region of 10–30 nm, the pore volume of CS-4 was considerably lower than that of g-C_3N_4. This difference indicates that the pores of g-C_3N_4 were blocked or occupied by CdS nanoparticles. Fig. 4**c** shows the absorption spectra of the samples. In the visible light region at 450↓650 nm, the absorption of g-C_3N_4 very weak, while that of CdS was stronger. Hence, the visible light absorption of CdS/g-C_3N_4 increased with the content of CdS in the sample. Then, the band gap energy (E_g) for the samples was determined through a Tauc plot, $(\alpha h\upsilon)^{1/n} = A(h\upsilon - E_g)$, where n is 2 for directly allowed transitions (Fig. 4d). The resulting values of E_g for CdS, g-C_3N_4, and CS-4 were 2.0, 2.61 and 2.1 eV, respectively. Moreover, the enhanced absorption of CS samples at wavelengths longer than 600 nm is probably due to the formation of a heterojunction between CdS and g-C_3N_4.

3.2. Photo electrochemical oxidation of H_2O

Fig. 5(a) shows the current-voltage diagrams of g-C_3N_4, CdS and CS-4 film electrodes in 0.5 M $NaClO_4$. In the dark, the electrode current was negligible. Under visible light, the electrode current was greatly

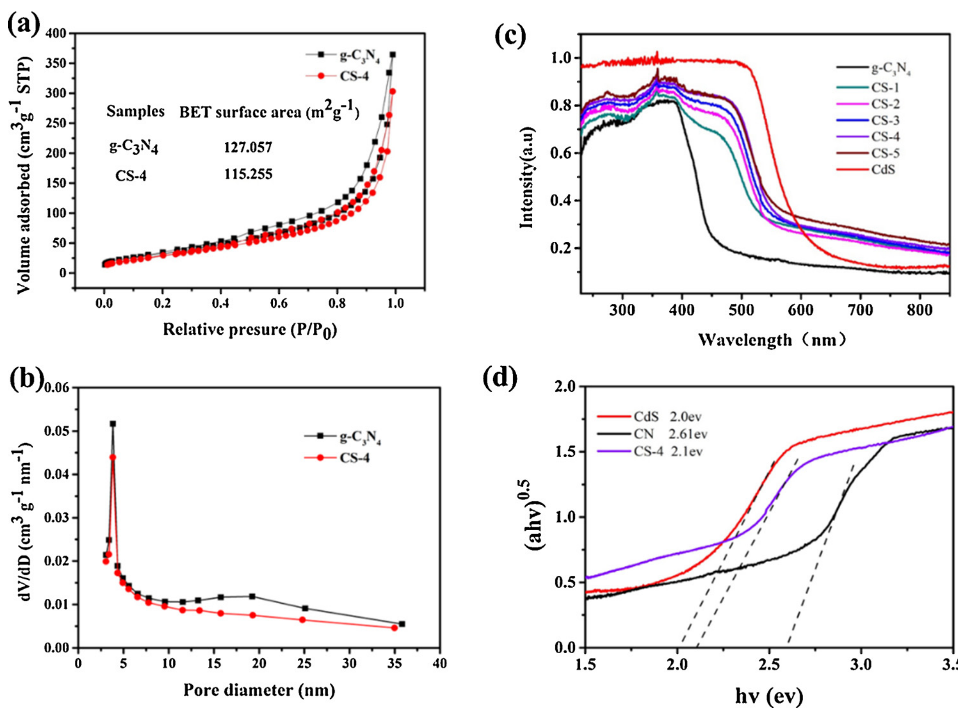

Fig. 4. N_2 adsorption/desorption isotherms (a), pore-size distributions (b), and UV–vis diffuse reflectance spectra measured from samples as indicated by the legends. Plot of $(ahv)^{0.5}$ vs hv (d).

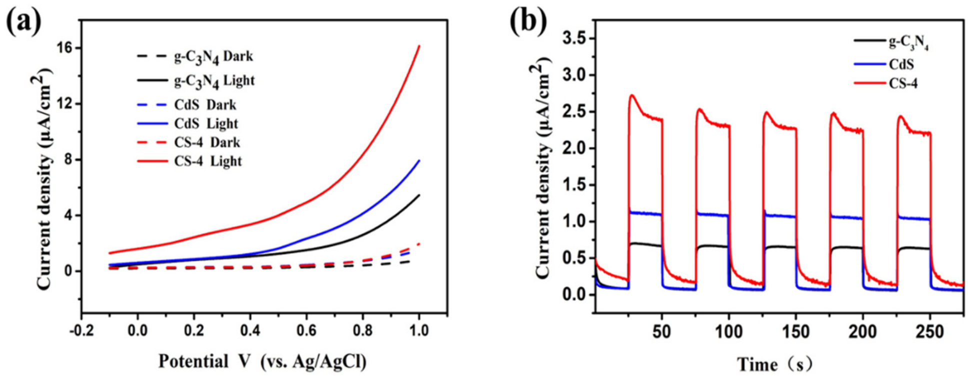

Fig. 5. Linear voltammetry curves for g-C_3N_4, CdS and CS-4 film electrodes (a), and the photocurrent at 0.4 V (vs. Ag/AgCl), measured in 0.5 M $NaClO_4$.

enhanced, indicative of water oxidation by the photo generated holes. During the positive potential sweep, the photocurrent increased due to the improved efficiency of charge separation. At a given potential, interestingly, the electrode photocurrent became larger in the order CS-4 > CdS > g-C_3N_4. Moreover, during the five repeated on/off light cycles, the transient photocurrent recorded at 0.4 V vs AgCl/Ag remained stable, and the CS-4 electrode had a photocurrent larger than the sum of the photocurrents measured from the CdS and g-C_3N_4 electrodes (Fig. 5b). The latter result is probably ascribed to the formation of a heterojunction between CdS and g-C_3N_4, promoting the separation of charge carriers and consequently increasing the hole oxidation of water. To further verify this hypothesis, the photoluminescence spectra (PL) of g-C_3N_4 and CS-4 were recorded. After excitation with 405 nm light, a strong and broad emission band was observed from g-C_3N_4, but not from CS-4 (Fig. S1a). Then, a time-resolved fluorescence spectrum was recorded (Fig. S1b). The decay curves of PL were well fitted to a tri-exponential function, from which the average lifetime of charge carriers was calculated (Table S1). Interestingly, CS-4 had an average lifetime of 4.24 ns, shorter than that of g-C_3N_4 (4.90 ns). These observations indicate that CdS and g-C_3N_4 form a heterojunction structure comprising the recombination of photo generated electrons and holes and consequently increasing the hole oxidation of water [54,55].

3.3. Photocatalytic evolution of H_2

Reactions were carried out at 6 °C by using lactic acid as a hole scavenger. Fig. 6a shows the result of H_2 production over different CS samples in aqueous suspensions, measured under visible light for 5 h. As the photo deposition time of CdS increased, the amount of H_2 initially increased and then decreased. A maximum amount of H_2 was observed from CS-4, with a value of 7746 μmol/g (reaction time is 3 h). Elemental analysis showed that the content of CdS in CS increased with photo deposition time and that CS-4 had 25.6 wt% CdS (Table 1). Notably, the CdS nanoparticles on the surface of the sample CS-5 were severely aggregated (Fig.S2). The reduced evolution of H_2 on CS-5 is due to the increased aggregation of CdS nanoparticles on the surface of g-C_3N_4 [43]. CS-4 was much more active than either CdS or g-C_3N_4 (Fig. 6b). 1 wt% Pt was loaded on the surface of the samples as a cocatalyst. Pure g-C_3N_4 had poor activity (1335 μmol g^{-1} in five hours), probably due to its weak absorption toward visible light (Fig. 4c). Pure CdS also exhibited poor activity (3135 μmol g^{-1} in five hours), probably due to its rapid recombination of charge carriers and its low stability against corrosion. After g-C_3N_4 was loaded with CdS, the composite materials showed excellent activity (12685 μmol g^{-1} in five hours). The activity of CS-4 was increased by approximately 9.5 and 4 times compared with those of g-C_3N_4 and CdS, respectively. When the cocatalyst did not be loaded on the surface of the samples, the hydrogen evolution performance of them was greatly reduced (Fig. S2). However, the hydrogen evolution performance of CS-4 (2133 μmol g^{-1} in five hour) is still much better than either g-C_3N_4 or CdS (364 μmol g^{-1} in five hour). The apparent quantum efficiency of CS-4 at 420 nm was 3.41% (see Supporting Information). To evaluate the stability and durability of CS-4, eleven repeated tests were performed, and the results are shown in Fig. 6c. After 55 h of continuous irradiation, CS-4 was still very active for the photocatalytic production of H_2. XRD analysis showed that CS-4 remained unchanged in the crystal structure (Fig. 6d). Importantly, the dissolved Cd^{2+} in aqueous solution was only 5.774 mg/L, much lower than the previously reported value (40 mg/L) [54]. Furthermore, a survey of the literature data illustrates that the present sample (CS-4) is competitive with the reported CdS/g-C_3N_4 samples in terms of hydrogen production and catalyst stability (Table S2). This high photocatalytic activity of CS-4 is attributed to the formation of a heterojunction between g-C_3N_4 and CdS. This results in the enhancement of visible light absorption and the efficiency of charge separation, consequently promoting the electron reduction of water to produce H_2.

3.4. Possible mechanism

To elucidate the mechanism of CS-4 photo catalysis, the energy positions of the conduction band (E_{CB}) and valence band (E_{VB}) were estimated with Eqs. (1) and (2), where χ is the element electronegativity and E_g is the band gap energy [47]. The χ values of CdS and g-C_3N_4 are 5.18 and 4.72 eV, respectively [56,57], whereas the E_g values of CdS and g-C_3N_4 are 2.0 and 2.61 eV, respectively (Fig. 4d). Accordingly, the calculated values of E_{CB} and E_{VB} for g-C_3N_4 are ↓1.15 and 1.42 V vs. normal hydrogen electrode (NHE), respectively. The calculated values of E_{CB} and E_{VB} for CdS are ↓0.36 and 1.74 V vs. NHE, respectively.

$$E_{CB} = \chi - E_c - 1/2E_g \tag{1}$$

$$E_{VB} = E_g + E_{CB} \tag{2}$$

Moreover, the flat band potentials (E_{fb}) for g-C_3N_4 and CS-4 were measured through Mott↓Schottky plots, and the results are shown in Fig. 7. With both g-C_3N_4 and CS-4, the plot slope was positive, indicating that the two solids were n-type semiconductors. The intercept with the x-axis was used to determine the E_{fb} values of g-C_3N_4 and CS-4, which were −1.13 and −0.38 V vs. Ag/AgCl, respectively. For n-type semiconductors, E_{CB} is approximately 0.2 V more negative than E_{fb} [58]. Then, the E_{CB} values of g-C_3N_4 and CS-4 are −1.13 and −0.38 V vs. NHE, respectively ($E_{NHE} = E_{Ag/AgCl} + 0.197$) [59,60]. According to E_g, the E_{VB} values for g-C_3N_4 and CS-4 are 1.48 and 1.72 V vs. NHE, respectively. The measured band edges are close to the calculated ones.

Based on the above calculations and experimental results, we explored the mechanism of electron transfer. In the literature, two types of heterojunctions have been proposed: Z-type and type II [35,61]. In the Z-type system (Fig. 8a), electron transfer occurs from photosystem II

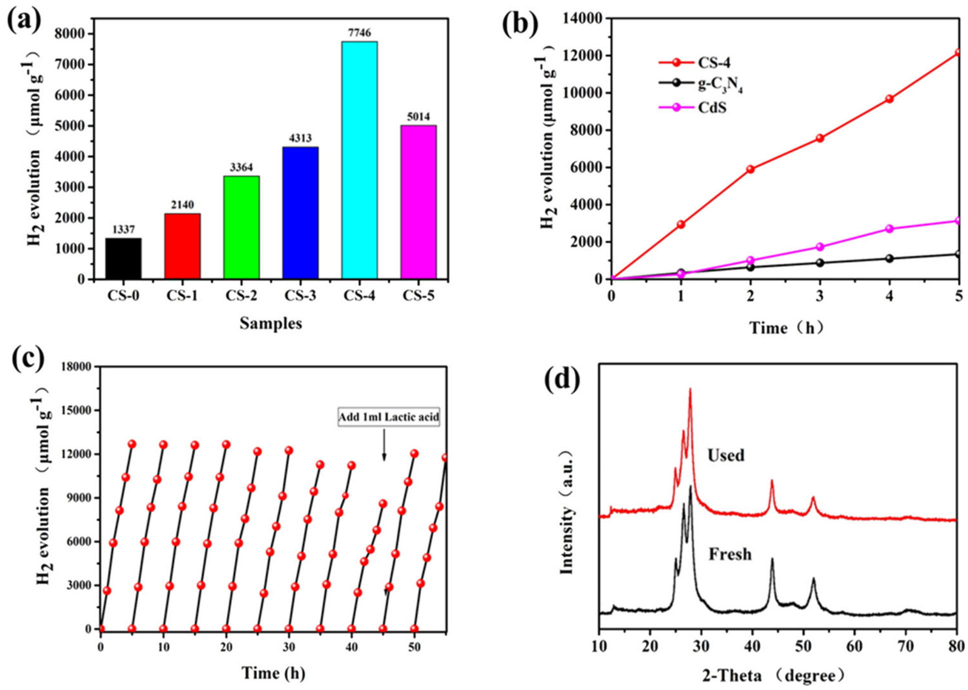

Fig. 6. Photocatalytic production of H_2 in an aqueous suspension containing lactic acid. Samples were (a) CS at 3 h, (b) g-C_3N_4, CdS, and CS-4, and (c) CS-4 (new lactic acid was added at 40 h). (d) XRD patterns of CS-4 before and after 55 h of the repeated test.

(CdS) to photosystem I (g-C_3N_4), resulting in recombination without neat redox reactions. Then, the holes remaining on CdS initiate the oxidation reaction and increase the light erosion of CdS, whereas the electrons remaining on g-C_3N_4 initiate the reduction reaction. In the type II system (Fig. 8b), electron transfer occurs from g-C_3N_4 to CdS, whereas hole transfer occurs from CdS to g-C_3N_4. Then, oxidation on g-C_3N_4 and reduction on CdS occur. In general, Pt is reduced from H_2PtCl_6 by photoelectrons on the semiconductor surface during photo deposition. Therefore, the site of photo generated electron flow can be characterized by observing the position of platinum nanoparticles. In the TEM and HRTEM images of Pt/CS-4 (Fig. 8c and d), there were two lattice fringe spacings at 0.330 and 0.229 nm, corresponding to the (002) plane of CdS and the (111) plane of Pt, respectively. A linear scan of EDX for specific regions (Fig. S4c) showed that the distribution of Pt is consistent with the distribution of Cd and S, which means that Pt nanoparticles are closely attached to the surface of the CdS and implies electron transfer from g-C_3N_4 to CdS. Similarly, photo generated holes can oxidize $MnSO_4$ to form MnOx, which can be used to characterizes the hole transfer route [62]. In the STEM image of CS-4, the substance that emitted a bright spot was CdS, and the layered substance near the edge belonged to MnOx. A linear scan of EDX for specific regions (Fig.S5) showed that the distribution of the Mn element was consistent with the distribution of O elements, which indicated the existence of MnOx nanoparticles. The distribution of Mn and O elements is generally consistent with the distribution of C and N elements. This further implies that the hole transfers from g-C_3N_4 to the site of MnOx nanoparticles, where the Mn^{2+} is oxidized by holes and forms MnOx. Such charge transfer results suggest that CS-4 operates with a type II mechanism. Under illumination, both g-C_3N_4 and CdS are excited. To achieve Fermi level balance, the conduction electrons of g-C_3N_4 are transferred to the conduction band of CdS, whereas the valence holes of CdS are transferred to the valence band of g-C_3N_4. As a result, both CdS and g-C_3N_4 have improved efficiency of charge separation and hence increased activity for water oxidation and reduction, respectively. Meanwhile, the photo corrosion of CdS due to the hole oxidation of $S^{2\downarrow}$ is suppressed, increasing the catalyst stability and activity for H_2 production.

4. Conclusions

A heterostructured CdS/g-C_3N_4 material has been successfully achieved through in situ photochemical deposition of CdS. The composite material shows significantly enhanced activity for hydrogen evolution under visible light. The photo catalyst also has superior stability and remains stable for up to 55 h. The enhanced activity and stability are due to an intimate heterojunction between CdS and g-C_3N_4,

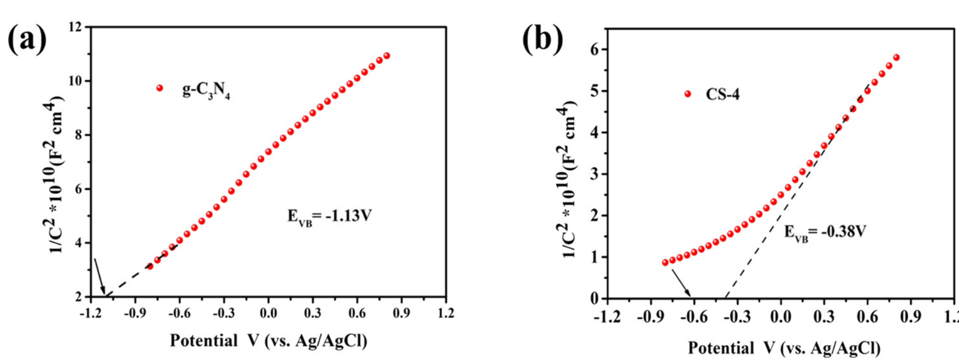

Fig. 7. Mott-Schottky plots of g-C_3N_4 and CS-4.

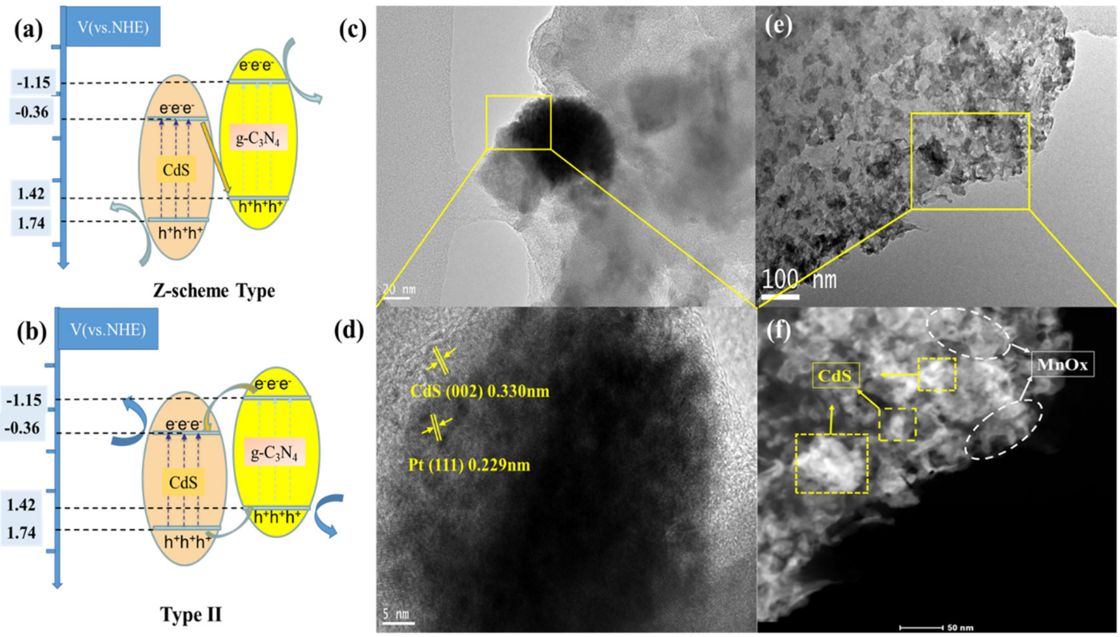

Fig. 8. Energy level diagrams and charge transfer routes of Z-type (a) and type II (b) CS-4. TEM (c) and HRTEM (d) of CS-4-Pt. TEM (e) and STEM (f) of CS-4 MnOx.

which facilitates band overlapping and promotes charge separation. This work provides a new method to precisely make an ideal heterojunction of CdS/g-C_3N_4.

Acknowledgement

This project was supported by the National Natural Science Foundation of China (Grant 21621005, 21537005, and 21425730), and the National Key Technology Research and Development Program of China (Grant 2018YFC1800705).

Appendix A. Supplementary data

Supplementary material related to this article can be found, in the online version, at doi:https://doi.org/10.1016/j.apcatb.2019.117848.

References

[1] R. Asahi, T. Morikawa, T. Ohwaki, K. Aoki, Y. Taga, Visible-light photocatalysis in nitrogen-doped titanium oxides, Science 293 (2001) 269–271.
[2] A. Fujishima, K. Honda, Electrochemical photolysis of water at a semiconductor electrode, Nature 238 (1972) 37–38.
[3] S. Kundu, A. Patra, Nanoscale strategies for light harvesting, Chem. Rev. 117 (2017) 712–757.
[4] W.-J. Ong, L.-L. Tan, Y.H. Ng, S.-T. Yong, S.-P. Chai, Graphitic carbon nitride (g-C_3N_4)-based photocatalysts for artificial photosynthesis and environmental remediation: are we a step closer to achieving sustainability? Chem. Rev. 116 (2016) 7159–7329.
[5] J. Wen, J. Xie, X. Chen, X. Li, A review on g-C_3N_4-based photocatalysts, Appl. Surf. Sci. 391 (2017) 72–123.
[6] H. Wang, L. Zhang, Z. Chen, J. Hu, S. Li, Z. Wang, J. Liu, X. Wang, Semiconductor heterojunction photocatalysts: design, construction, and photocatalytic performances, Chem. Soc. Rev. 43 (2014) 5234–5244.
[7] X. Wang, K. Maeda, A. Thomas, K. Takanabe, G. Xin, J.M. Carlsson, K. Domen, M. Antonietti, A metal-free polymeric photocatalyst for hydrogen production from water under visible light, Nat. Mater. 8 (2008) 76–80.
[8] G. Mamba, A.K. Mishra, Graphitic carbon nitride (g-C_3N_4) nanocomposites: a new and exciting generation of visible light driven photo catalysts for environmental pollution remediation, Appl. Catal. B 198 (2016) 347–377.
[9] Y. Zhang, T. Mori, L. Niu, J. Ye, Non-covalent doping of graphitic carbon nitride polymer with graphene: controlled electronic structure and enhanced optoelectronic conversion, Energy Environ. Sci. 4 (2011) 4517–4521.
[10] Y. Hong, C. Li, D. Li, Z. Fang, B. Luo, X. Yan, H. Shen, B. Mao, W. Shi, Precisely tunable thickness of graphitic carbon nitride nanosheets for visible-light-driven photocatalytic hydrogen evolution, Nanoscale 9 (2017) 14103–14110.
[11] S. Guo, Y. Tang, Y. Xie, C. Tian, Q. Feng, W. Zhou, B. Jiang, P-doped tubular g-C_3N_4 with surface carbon defects: universal synthesis and enhanced visible-light photocatalytic hydrogen production, Appl. Catal. B 218 (2017) 664–671.
[12] C. Zhou, C. Lai, D. Huang, G. Zeng, C. Zhang, M. Cheng, L. Hu, J. Wan, W. Xiong, M. Wen, X. Wen, L. Qin, Highly porous carbon nitride by supramolecular preassembly of monomers for photocatalytic removal of sulfamethazine under visible light driven, Appl. Catal. B 220 (2018) 202–210.
[13] Q. Xiang, J. Yu, M. Jaroniec, Preparation and enhanced visible-light photocatalytic H_2-production activity of graphene/C_3N_4 composites, J. Phys. Chem. C 115 (2011) 7355–7363.
[14] J. Wang, Z. Yang, X. Gao, W. Yao, W. Wei, X. Chen, R. Zong, Y. Zhu, Core-shell g-C_3N_4@ZnO composites as photoanodes with double synergistic effects for enhanced visible-light photoelectrocatalytic activities, Appl. Catal. B 217 (2017) 169–180.
[15] G. Liu, P. Niu, C. Sun, S.C. Smith, Z. Chen, G.Q. Lu, H.-M. Cheng, Unique electronic structure induced high photoreactivity of sulfur-doped graphitic C_3N_4, J. Am. Chem. Soc. 132 (2010) 11642–11648.
[16] Y. Lu, X. Cheng, G. Tian, H. Zhao, L. He, J. Hu, S.-M. Wu, Y. Dong, G.-G. Chang, S. Lenaerts, S. Siffert, G. Van Tendeloo, Z.-F. Li, L.-L. Xu, X.-Y. Yang, B.-L. Su, Hierarchical CdS/m-TiO_2/G ternary photocatalyst for highly active visible light-induced hydrogen production from water splitting with high stability, Nano Energy 47 (2018) 8–17.
[17] H. Tada, T. Mitsui, T. Kiyonaga, T. Akita, K. Tanaka, All-solid-state Z-scheme in CdS–Au–TiO_2 three-component nanojunction system, Nat. Mater. 5 (2006) 782.
[18] R. Shi, H.F. Ye, F. Liang, Z. Wang, K. Li, Y. Weng, Z. Lin, W.F. Fu, C.M. Che, Y. Chen, Interstitial p-doped CdS with long-lived photogenerated electrons for photocatalytic water splitting without sacrificial agents, Adv Mater 30 (2018) 1705941.
[19] L. Zhang, F. Sun, Y. Zuo, C. Fan, S. Xu, S. Yang, F. Gu, Immobilisation of CdS nanoparticles on chitosan microspheres via a photochemical method with enhanced photocatalytic activity in the decolourisation of methyl orange, Appl. Catal. B 156–157 (2014) 293–300.
[20] Y.P. Xie, Z.B. Yu, G. Liu, X.L. Ma, H.-M. Cheng, CdS–mesoporous ZnS core–shell particles for efficient and stable photocatalytic hydrogen evolution under visible light, Energy Environ. Sci. 7 (2014) 1895–1901.
[21] J. Mort, W.E. Spear, Hole drift mobility and lifetime in CdS crystals, Phys. Rev. Lett. 8 (1962) 314–315.
[22] P. Chandran, P. Kumari, S. Sudheer Khan, Photocatalytic activation of CdS NPs under visible light for environmental cleanup and disinfection, Sol. Energy 105 (2014) 542–547.
[23] K. Wu, H. Zhu, Z. Liu, W. Rodríguez-Córdoba, T. Lian, Ultrafast charge separation and long-lived charge separated state in photocatalytic CdS–Pt nanorod heterostructures, J. Am. Chem. Soc. 134 (2012) 10337–10340.
[24] M. Osada, T. Sasaki, Two-dimensional dielectric nanosheets: novel nanoelectronics from nanocrystal building blocks, Adv. Mater. 24 (2012) 210–228.
[25] Y. Guo, L. Jiang, L. Wang, X. Shi, Q. Fang, L. Yang, F. Dong, C. Shan, Facile synthesis of stable cadmium sulfide quantum dots with good photocatalytic activities under stabilization of hydrophobic amino acids, Mater. Lett. 74 (2012) 26–29.
[26] D. Wang, D. Li, L. Guo, F. Fu, Z. Zhang, Q. Wei, Template-Free hydrothermal synthesis of novel three-dimensional dendritic CdS nanoarchitectures, J. Phys. Chem. C 113 (2009) 5984–5990.
[27] S. Qu, J. Huang, J. Yu, G. Chen, W. Hu, M. Yin, R. Zhang, S. Chu, C. Li, Ni_3S_2 nanosheet flowers decorated with CdS quantum dots as a highly active electrocatalysis electrode for synergistic water splitting, ACS Appl. Mater. Interfaces 9 (2017) 29660–29668.
[28] S. Hoang, S.P. Berglund, R.R. Fullon, R.L. Minter, C.B. Mullins, Chemical bath deposition of vertically aligned TiO_2 nanoplatelet arrays for solar energy conversion

applications, J. Mater. Chem. A 1 (2013) 4307–4315.
[29] K.S. Suslick, S.-B. Choe, A.A. Cichowlas, M.W. Grinstaff, Sonochemical synthesis of amorphous iron, Nature 353 (1991) 414–416.
[30] S. Qian, C. Wang, W. Liu, Y. Zhu, W. Yao, X. Lu, An enhanced CdS/TiO_2 photocatalyst with high stability and activity: effect of mesoporous substrate and bifunctional linking molecule, J. Mater. Chem. 21 (2011) 4945–4952.
[31] X.-H. Lu, S.-L. Xie, T. Zhai, Y.-F. Zhao, P. Zhang, Y.-L. Zhang, Y.-X. Tong, Monodisperse CeO_2/CdS heterostructured spheres: one-pot synthesis and enhanced photocatalytic hydrogen activity, RSC Adv. 1 (2011) 1207–1210.
[32] Y. Wu, H. Wang, W. Tu, S. Wu, Y. Liu, Y.Z. Tan, H. Luo, X. Yuan, J.W. Chew, Petal-like CdS nanostructures coated with exfoliated sulfur-doped carbon nitride via chemically activated chain termination for enhanced visible-light–driven photocatalytic water purification and H_2 generation, Appl. Catal. B 229 (2018) 181–191.
[33] J. Fu, B. Chang, Y. Tian, F. Xi, X. Dong, Novel C_3N_4–CdS composite photocatalysts with organic–inorganic heterojunctions: in situ synthesis, exceptional activity, high stability and photocatalytic mechanism, J. Mater. Chem. A 1 (2013) 3083–3090.
[34] Y. Li, X. Wei, H. Li, R. Wang, J. Feng, H. Yun, A. Zhou, Fabrication of inorganic–organic core–shell heterostructure: novel CdS@g-C_3N_4 nanorod arrays for photoelectrochemical hydrogen evolution, RSC Adv. 5 (2015) 14074–14080.
[35] S.-W. Cao, Y.-P. Yuan, J. Fang, M.M. Shahjamali, F.Y.C. Boey, J. Barber, S.C. Joachim Loo, C. Xue, In-situ growth of CdS quantum dots on g-C_3N_4 nanosheets for highly efficient photocatalytic hydrogen generation under visible light irradiation, Int. J. Hydrogen Energy 38 (2013) 1258–1266.
[36] Y. Cui, In-situ synthesis of C_3N_4/CdS composites with enhanced photocatalytic properties, Chinese J. Catal. 36 (2015) 372–379.
[37] Z. Xu, H. Li, Z. Wu, J. Sun, Z. Ying, J. Wu, N. Xu, Enhanced charge separation of vertically aligned CdS/g-C_3N_4 heterojunction nanocone arrays and corresponding mechanisms, J. Mater. Chem. C 4 (2016) 7501–7507.
[38] D. Zheng, G. zhang, X. Wang, Integrating CdS quantum dots on hollow graphitic carbon nitride nanospheres for hydrogen evolution photocatalysis, Appl. Catal. B 179 (2015) 479–488.
[39] W.-K. Jo, N.C.S. Selvam, Z-scheme CdS/g-C_3N_4 composites with RGO as an electron mediator for efficient photocatalytic H $_2$ production and pollutant degradation, Chem. Eng. J. 317 (2017) 913–924.
[40] P. Chen, F. Liu, H. Ding, S. Chen, L. Chen, Y.-J. Li, C.-T. Au, S.-F. Yin, Porous double-shell CdS@C_3N_4 octahedron derived by in situ supramolecular self-assembly for enhanced photocatalytic activity, Appl. Catal. B 252 (2019) 33–40.
[41] R. Li, F. Zhang, D. Wang, J. Yang, M. Li, J. Zhu, X. Zhou, H. Han, C. Li, Spatial separation of photogenerated electrons and holes among {010} and {110} crystal facets of BiVO4, Nat. Commun. 4 (2013) 1432.
[42] K. Wenderich, G. Mul, Methods, mechanism, and applications of photodeposition in photocatalysis: a review, Chem. Rev. 116 (2016) 14587–14619.
[43] H. Zhao, H. Zhang, G. Cui, Y. Dong, G. Wang, P. Jiang, X. Wu, N. Zhao, A photochemical synthesis route to typical transition metal sulfides as highly efficient cocatalyst for hydrogen evolution: from the case of NiS/g-C_3N_4, Appl. Catal. B 225 (2018) 284–290.
[44] H. Tada, M. Fujishima, H. Kobayashi, Photodeposition of metal sulfide quantum dots on titanium(IV) dioxide and the applications to solar energy conversion, Chem. Soc. Rev. 40 (2011) 4232–4243.
[45] Y. Li, H. Wang, S. Peng, Tunable photodeposition of MoS_2 onto a composite of reduced graphene oxide and CdS for synergic photocatalytic hydrogen generation, J. Phys. Chem. C 118 (2014) 19842–19848.
[46] T. Takata, C. Pan, M. Nakabayashi, N. Shibata, K. Domen, Fabrication of a core-shell-type photocatalyst via photodeposition of group IV and V transition metal oxyhydroxides: an effective surface modification method for overall water splitting, J. Am. Chem. Soc. 137 (2015) 9627–9634.
[47] W. Jiang, X. Zong, L. An, S. Hua, X. Miao, S. Luan, Y. Wen, F.F. Tao, Z. Sun, Consciously constructing heterojunction or direct Z-scheme photocatalysts by regulating electron flow direction, ACS Catal. 8 (2018) 2209–2217.
[48] J. Zhu, F. Fan, R. Chen, H. An, Z. Feng, C. Li, Direct imaging of highly anisotropic photogenerated charge separations on different facets of a single $BiVO_4$ Photocatalyst, Angew. Chem. Int. Ed. Engl. 54 (2015) 9111–9114.
[49] L. Mu, Y. Zhao, A. Li, S. Wang, Z. Wang, J. Yang, Y. Wang, T. Liu, R. Chen, J. Zhu, F. Fan, R. Li, C. Li, Enhancing charge separation on high symmetry $SrTiO_3$ exposed with anisotropic facets for photocatalytic water splitting, Energy Environ. Sci. 9 (2016) 2463–2469.
[50] M. Fujii, K. Nagasuna, M. Fujishima, T. Akita, H. Tada, Photodeposition of CdS quantum dots on TiO_2: preparation, characterization, and reaction mechanism, J. Phys. Chem. C 113 (2009) 16711–16716.
[51] W. Li, C. Feng, S. Dai, J. Yue, F. Hua, H. Hou, Fabrication of sulfur-doped g-C_3N_4/Au/CdS Z-scheme photocatalyst to improve the photocatalytic performance under visible light, Appl. Catal. B 168–169 (2015) 465–471.
[52] Y. Xu, Y. Chen, W.-F. Fu, Visible-light driven oxidative coupling of amines to imines with high selectivity in air over core-shell structured CdS@C_3N_4, Appl. Catal. B 236 (2018) 176–183.
[53] J. Chu, X. Li, J. Qi, Hydrothermal synthesis of CdS microparticles–graphene hybrid and its optical properties, CrystEngComm 14 (2012) 1881–1884.
[54] C. Li, Y. Du, D. Wang, S. Yin, W. Tu, Z. Chen, M. Kraft, G. Chen, R. Xu, Unique P–Co–N surface bonding states constructed on g-C_3N_4 nanosheets for drastically enhanced photocatalytic activity of H_2 evolution, Adv. Funct. Mater. 27 (2017).
[55] J. Cai, J. Huang, S. Wang, J. Iocozzia, Z. Sun, J. Sun, Y. Yang, Y. Lai, Z. Lin, Crafting mussel-inspired metal nanoparticle-decorated ultrathin graphitic carbon nitride for the degradation of chemical pollutants and production of chemical resources, Adv Mater 31 (15) (2019) 1806314.
[56] K. Dai, L. Lu, C. Liang, Q. Liu, G. Zhu, Heterojunction of facet coupled g-C_3N_4/surface-fluorinated TiO_2 nanosheets for organic pollutants degradation under visible LED light irradiation, Appl. Catal. B 156–157 (2014) 331–340.
[57] X. Yue, S. Yi, R. Wang, Z. Zhang, S. Qiu, Cadmium sulfide and nickel synergetic cocatalysts supported on graphitic carbon nitride for visible-light-driven photocatalytic hydrogen evolution, Sci. Rep. 6 (2016) 22268.
[58] Z. Qin, Y. Chen, Z. Huang, J. Su, L. Guo, A bifunctional NiCoP-based core/shell cocatalyst to promote separate photocatalytic hydrogen and oxygen generation over graphitic carbon nitride, J. Mater. Chem. A 5 (2017) 19025–19035.
[59] G. Ai, H. Li, S. Liu, R. Mo, J. Zhong, Solar water splitting by TiO_2/CdS/Co–Pi nanowire array photoanode enhanced with Co–Pi as hole transfer relay and CdS as light absorber, Adv. Funct. Mater. 25 (2015) 5706–5713.
[60] J. Xu, Y. Qi, L. Wang, In situ derived Ni_2P/Ni encapsulated in carbon/g-C_3N_4 hybrids from metal–organic frameworks/g-C_3N_4 for efficient photocatalytic hydrogen evolution, Appl. Catal. B 246 (2019) 72–81.
[61] W.-K. Jo, N.C.S. Selvam, Z-scheme CdS/g-C_3N_4 composites with RGO as an electron mediator for efficient photocatalytic H_2 production and pollutant degradation, Chem. Eng. J. 317 (2017) 913–924.
[62] Y. Wang, Z. Zhang, L. Zhang, Z. Luo, J. Shen, H. Lin, J. Long, J.C.S. Wu, X. Fu, X. Wang, C. Li, Visible-light driven overall conversion of CO_2 and H_2O to CH_4 and O_2 on 3D-SiC@2D-MoS_2 heterostructure, J. Am. Chem. Soc. 140 (2018) 14595–14598.